Applied Numerical Modeling in Geomechanics – 2020 – Billaux, Hazzard, Nelson & Schöpfer (eds.) Paper: 12-04

Anisotropic permeability in the EDZ of drifts in rock salt – A numerical approach

Christian Missal[1] & Joachim Stahlmann[2]
[1] *Itasca Consultants GmbH, Gelsenkirchen, Germany*
[2] *Institute for Soil Mechanics and Foundation Engineering, TU Braunschweig, Braunschweig, Germany*

1 INTRODUCTION

Salt deposits are regarded as potential sites for the disposal of radioactive waste. In principle, risks to the biosphere should be minimized by underground storage. For this reason, the radioactive waste should be enclosed as permanently as possible and the transport of harmful substances into the biosphere should be prevented or delayed. Rock salt can be regarded as impermeable in its intact state. During the excavation of drifts in the rock salt, an excavation damaged zone (EDZ) develops in the area close to the drift due to stress redistribution, which develops as an anisotropic crack network. For permanent containment, the potential disposal areas are separated by sealing structures, so that the functionality of these geotechnical barriers are of particular importance. Integral permeability is a measure of functionality. The integral permeability follows from the hydraulic resistances of the intact rock salt, the EDZ, the contact zone and the sealing structure, whereby the contact zone and the EDZ initially dominate the integral permeability and represent a potential path for fluids.

The interaction of damage, fluid pressure and stress state thus influence the permeability in the EDZ. In the following, a concept is presented which can describe the flow through the EDZ normal and tangential to the drift contour in a continuum mechanical approach. Since the crystalline nature of the rock salt forms a crack network similar to a jointed water conductor on the micro scale, the rock mechanical approaches of Louis (1967) and Rodatz (1973) are adapted.

2 DEVELOPMENT OF ANISOTROPIC PERMEABILITY

Due to a stress state above the dilatancy boundary, damage-induced strains occur in the drift contour (Fig. 1). It should be noted that mechanical sign conventions are used instead of geotechnical sign conventions (cf. Missal, 2019). For example, the radial damage-induced strains lead to cracks that run tangentially around the drift. The principal permeability results from the two orthogonally oriented components of the damage-induced strains (Missal 2019).

In order to determine the particular direction-dependent permeability, a crack spectrum must first be determined. With the density function (Eq. 1) of the *Rayleigh* distribution, a standardized crack spectrum without negative crack widths can be calculated for each principal damage component.

$$\mathrm{D}(x^*, \underline{\sigma}) = \begin{cases} \frac{x^*}{\underline{\sigma}^2} \mathrm{e}^{-\frac{x^{*2}}{2\underline{\sigma}^2}} & \text{für } x > 0 \ \wedge \ \underline{\sigma} > 0 \\ 0 & \text{für } x \leq 0 \ \vee \ \underline{\sigma} \leq 0 \end{cases} \tag{1}$$

where x^* crack width in µm, $\underline{\sigma}$ shape parameter in µm

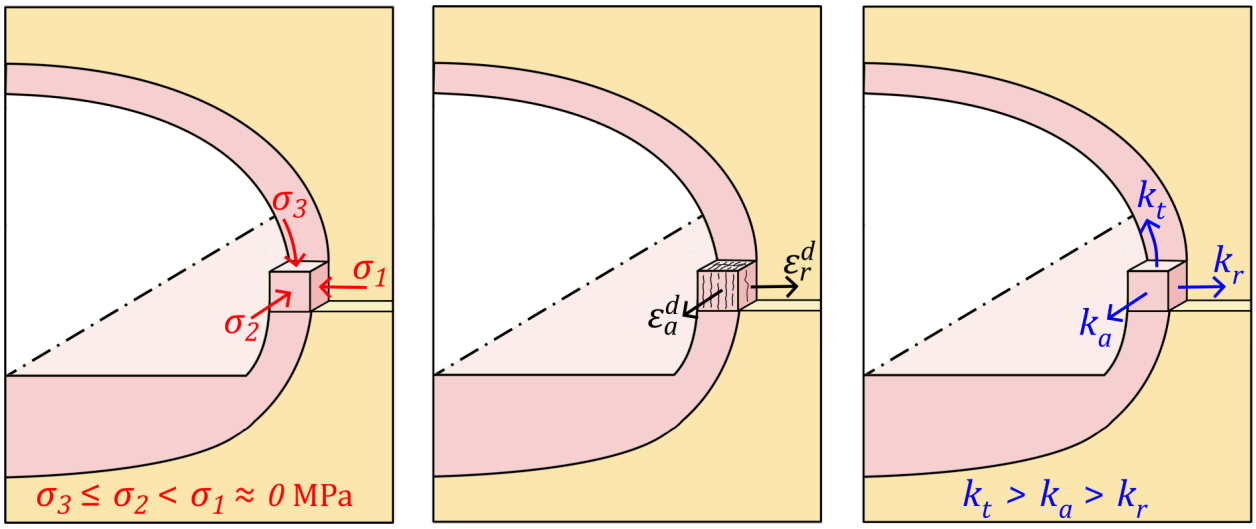

Figure 1. Relationship between stress state, direction of damage-induced strains and resulting anisotropic permeability in the EDZ of the drift contour.

Crack permeability according to the equation 2 can be determined for each crack width, taking parallel or non-parallel flow into account. The crack permeability is determined by the crack width, the crack distance and the surface condition of the crack. The crack width can also be influenced by the effective fluid pressure and the crack normal stress.

$$\mathrm{k}(x) = \kappa \cdot \frac{\langle 2x \rangle^3}{12 \cdot \overline{b}_K \cdot \left(1 + 8{,}8 \cdot \mathrm{H}\left(\frac{\overline{d}_r}{d_H^*} - 0{,}032\right) \cdot \left(\frac{\overline{d}_r}{d_H^*}\right)^{\frac{3}{2}}\right)} \tag{2}$$

where $\mathrm{k}(x)$ crack permeability in m², κ degree of separation, $2x$ crack width in m, $\overline{b}_K$ mean crack distance in m, $\mathrm{H}(\ldots)$ *Heaviside* step function, $\overline{d}_r$ mean absolute roughness in m, d_H^* hydraulic diameter where $d_H^* = 4x$ in m

Permeability can only become effective with connected pathways due to crack cross-linking. The occurrence of crack cross-linking is determined with a Föppl function (Eq. 3). Below the crack cross-linking threshold the function assumes the value 0, while above the crack cross-linking threshold the function value is returned. This ensures that only continuous pathways successively contribute to an increase in permeability.

$$\left\{\mathrm{P}\left(\varepsilon_v^d, \varepsilon_i^d\right)\right\} = \left\{\left\langle \frac{\varepsilon_v^d \cdot (1 + p_1 \cdot \varepsilon_i^d)}{\varepsilon_{v,B}^d} - p_c \right\rangle\right\} \tag{3}$$

where ε_v^d damage-induced dilatancy, ε_i^d damage-induced principal strain (i = *1, 2, 3*), $\varepsilon_{v,B}^d$ failure dilatancy, p_1 scaling parameter, p_c crack cross-link threshold

The principal permeability is determined by the interaction of the crack spectrum, the crack permeability for the particular crack width, and the crack cross-linking (Eq. 4). The primitive is unknown for this integral for the calculation of permeability. Therefore, it is solved in the implementation by numerical integration.

$$\begin{Bmatrix} k_1 \\ k_2 \\ k_3 \end{Bmatrix} = k_{ini} + \begin{Bmatrix} \int_0^\infty \left(\mathrm{P}(\varepsilon_v^d, \varepsilon_2^d) \cdot \mathrm{D}\left(x^*, \underline{\sigma}(\varepsilon_2^d)\right) \cdot \mathrm{k}(x) + \mathrm{P}(\varepsilon_v^d, \varepsilon_3^d) \cdot \mathrm{D}\left(x^*, \underline{\sigma}(\varepsilon_3^d)\right) \cdot \mathrm{k}(x)\right) \mathrm{d}x \\ \int_0^\infty \left(\mathrm{P}(\varepsilon_v^d, \varepsilon_3^d) \cdot \mathrm{D}\left(x^*, \underline{\sigma}(\varepsilon_3^d)\right) \cdot \mathrm{k}(x) + \mathrm{P}(\varepsilon_v^d, \varepsilon_1^d) \cdot \mathrm{D}\left(x^*, \underline{\sigma}(\varepsilon_1^d)\right) \cdot \mathrm{k}(x)\right) \mathrm{d}x \\ \int_0^\infty \left(\mathrm{P}(\varepsilon_v^d, \varepsilon_1^d) \cdot \mathrm{D}\left(x^*, \underline{\sigma}(\varepsilon_1^d)\right) \cdot \mathrm{k}(x) + \mathrm{P}(\varepsilon_v^d, \varepsilon_2^d) \cdot \mathrm{D}\left(x^*, \underline{\sigma}(\varepsilon_2^d)\right) \cdot \mathrm{k}(x)\right) \mathrm{d}x \end{Bmatrix} \tag{4}$$

where k_i total principal permeability in m² (i = *1, 2, 3*), k_{ini} initial permeability where $k_{ini} = 1 \cdot 10^{-23}$ in m².

The implementation for *FLAC3D* (Itasca 2017) is done for the constitutive model *TUBSsalt.* This constitutive model can describe the stress-time-deformation behavior for rock salt under consideration of damage and healing. The material model is described in Gährken et al. (2015, 2018).

3 ANISOTROPIC PERMEABILITY IN THE EDZ OF A GENERIC DRIFT

Based on Missal et al. (2015), the anisotropic damage development and the resulting permeabilities are shown for a generic drift in rock salt (cf. Missal 2019). The dimensions of the numerical model are 60 m in width, 8 m in depth and 75 m in height. The drift in the form of a mouth profile, which is oriented to a typical cross-section of a drift in a repository, has a width of about 10 m and a height of about 5 m. The bottom of the drift is at a depth of 600 m, so that a stress boundary condition of 14 MPa is applied at the upper edge of the model. The remaining model edges are kept normal to the edge with displacement boundary conditions. The simulation includes the initial stress state, the excavation of the drift and an open standing time of the drift of 25 years. The simulation was carried out with *FLAC3D* Version 6.0.

Figure 2 shows the distribution of the damage-induced strain components at the time 25 years after excavation. In the blue areas the particular component is compressed, in the red areas an extension is calculated. The legend is scaled to ±1‰. In the impact of the drift, cracks increasingly develop in the axial direction, so that there is a possibility of crack cross-linking with the tangential cracks and a potential site of access for solution into the EDZ is formed.

Taking into account the damage-induced strain components and the normal stress acting on the crack surfaces an anisotropic permeability tensor results around the contour. The highest principal permeability is tangential permeability, since this is influenced by axial and radial damage. The lowest permeability is in the radial direction due to only axial damage. For the flow along the EDZ of the drift, the axial permeability is the key parameter, whereby it is only slightly less than the tangential permeability. The possible solution access from the drift into the crack system, however, is limited by the radial permeability.

Further calculation results and a complete description of parameters and boundary conditions can be found in Missal (2019).

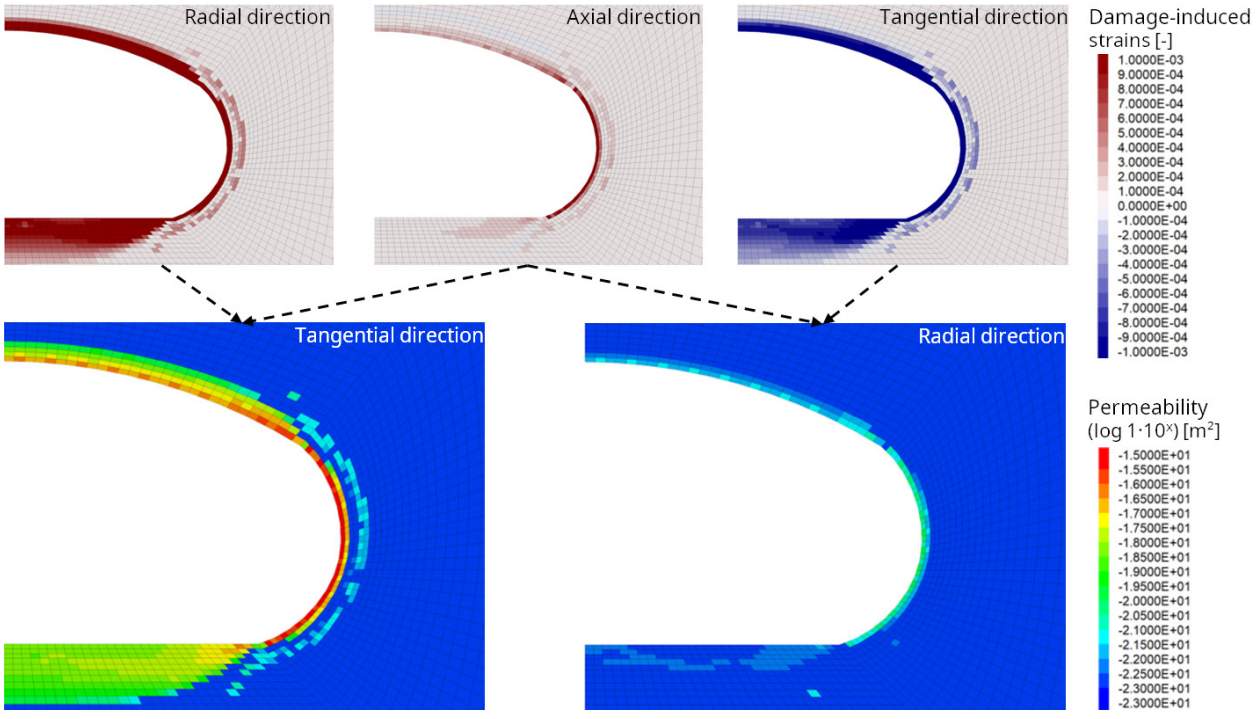

Figure 2. Damage-induced strains and resulting tangential or radial permeability at an open drift in rock salt after 25 years of open standing time.

4 CONCLUSIONS

Due to a three-dimensional stress state above the dilatancy boundary around a drift an EDZ with anisotropic damage occurs. The developing crack network favors a flow parallel to the drift contour. The constitutive model *TUBSsalt* calculates the damage-induced dilatancy from the damage-induced strain components so that a statement can be made about the magnitude and direction of the damage. Based on these quantities, crack width spectra are calculated with a *Rayleigh* distribution. In addition, crack permeability can be determined for each crack width, taking parallel or non-parallel flow into account. The permeability results from the integral of the crack width spectrum linked to the crack permeability. The total permeability in a principal direction results from the sum of the particular functions of the two damage parts orthogonally oriented to this direction.

The development of anisotropic permeability over time was shown using a generic drift as an example. In comparison to the isotropic permeability, a higher permeability is obtained parallel to the drift, while the radial permeability limiting the solution access is smaller. The presented approach is still to be validated by laboratory experiments and calibrated by in-situ measurements.

REFERENCES

Gährken, A., DeVries, K.L. & Stahlmann, J. 2018. Advanced development of the constitutive model TUBSsalt for rock salt regarding the influence of Lode angle effects; In: Fahland, S.; Hammer, J.; Hansen, F.; Heusermann, S.; Lux, K.-H.; Minkley, W. (Eds.): *Mechanical behavior of Salt IX*. Federal Institute for Geosciences and Natural Resources (BGR), Hannover.

Gährken, A., Missal, C. & Stahlmann, J. 2015. A thermal-mechanical constitutive model to describe deformation, damage and healing of rock salt. In: Roberts, L.; Mellegard, K.; Hansen, F. (Ed.): *Mechanical behavior of Salt VIII*, Pp. 331-338. Taylor & Francis, London.

Itasca Consulting Group, Inc. 2017. *FLAC3D – Fast Lagrangian Analysis of Continua in Three-Dimensions, Ver. 6.0*. Minneapolis.

Louis, C. 1967. Strömungsvorgänge in klüftigen Medien und ihre Wirkung auf die Standsicherheit von Bauwerken und Böschungen im Fels. TH Karlsruhe, Fakultät für Bauingenieur- und Vermessungswesen, Dissertation. Karlsruhe.

Missal, C. 2019. Numerisches Modell zur Entwicklung der Permeabilität von Steinsalz in Abhängigkeit von Schädigung, Fluiddruck und Spannungszustand. TU Braunschweig, Fakultät Architektur, Bauingenieurwesen und Umweltwissenschaften, Dissertation, Braunschweig.

Missal, C., Gährken, A. & Stahlmann, J. 2015. Numerical investigations on the anisotropic damage of the EDZ of drifts in rock salt. In: Roberts, L.; Mellegard, K.; Hansen, F. (Hrsg.): *Mechanical behavior of Salt VIII*, Pp. 109-114. Taylor & Francis, London.

Rodatz, W. 1973. Berechnung räumlicher, hydraulisch-mechanischer Wechselwirkungen im klüftigen Fels. TH Karlsruhe, Fakultät für Bauingenieur- und Vermessungswesen, Dissertation. Karlsruhe.